RSC Advances

This is an *Accepted Manuscript*, which has been through the Royal Society of Chemistry peer review process and has been accepted for publication.

Accepted Manuscripts are published online shortly after acceptance, before technical editing, formatting and proof reading. Using this free service, authors can make their results available to the community, in citable form, before we publish the edited article. This *Accepted Manuscript* will be replaced by the edited, formatted and paginated article as soon as this is available.

You can find more information about *Accepted Manuscripts* in the Information for Authors.

Please note that technical editing may introduce minor changes to the text and/or graphics, which may alter content. The journal's standard Terms & Conditions and the Ethical guidelines still apply. In no event shall the Royal Society of Chemistry be held responsible for any errors or omissions in this *Accepted Manuscript* or any consequences arising from the use of any information it contains.

ROYAL SOCIETY OF CHEMISTRY

www.rsc.org/advances

Activated carbon from *Luffa cylindrica* doped chitosan for mitigation of lead (II) from aqueous solution

Asha H. Gedam[a*], Rajendra S. Dongre[b]

[a*]Department of Allied Science, Cummins college of Engineering for Women, Nagpur- 441 110, India.

[b] Post Graduate Teaching Department of Chemistry, Rashtrasant Tukdoji Maharaj Nagpur University, Nagpur- 440 033, India.

E-mail: agedam.ccoew@gmail.com; Fax: 07104-280304, Mobile: (+91) 9730184638.

Abstract

The present study is concerned with the batch adsorption of toxic lead (II) ions from aqueous solution by using activated carbon of *Luffa cylindrica* fibers doped chitosan (ACLFCS) biocomposite as an adsorbent. The adsorption experiments were conducted as a function of pH, agitation time, initial lead (II) ion concentration and adsorbent doses. The synthesized biosorbent was characterized by instrumental techniques like XRD, FTIR, SEM, BET surface area and BJH pore size distribution. XRD analysis revealed that the synthesized ACLFCS adsorbent exhibited broad diffraction peaks with amorphous structure. The FTIR study shown the various functionalities such as C=O, -OH and $-NH_2$ responsible for lead (II) adsorption on ACLFCS biocomposite. The surface morphology of ACLFCS adsorbent possesses porous texture with round and elliptical shaped voids that can provide the adsorption sites to the adsorbate. The BJH pore size distribution analysis shown that the average pore diameter > 2 nm for all chitosan (CS), activated carbon of *Luffa cylindrica* (ACLF) and ACLFCS adsorbents, corresponds to the presence of mesoporous structure. The batch adsorption of Lead (II) ions has been carried out at room temperature where the optimum conditions for the maximum adsorption of lead (II) ions were attained at pH 5 with adsorbent dose of 0.1 g/L. The equilibrium adsorption isotherm data were fitted by the Langmuir and Freundlich models and Langmuir isotherm exhibited best fit with the experimental data. The maximum removal of lead (II) obtained 98% (experimental) and 112 mg/g (from Langmuir isotherm model). The adsorption kinetics was evaluated by pseudo first order, Pseudo second order and intraparticle diffusion models. The adsorption data well follows pseudo second order kinetic model. The high uptake of lead (II) ions using ACLFCS suggests an effective and low cost adsorbent for the treatment of water contaminated with lead (II) ions.

Keywords: Chitosan; *Luffa cylindrica*; Activated carbon; lead (II); Adsorption; Isotherm; Kinetics.

RSC Advances Accepted Manuscript

1. Introduction

The presence of lead in water, air and soil environment even in traces has detrimental effects on plants and animals. The natural sources of lead are soil erosion, volcanic eruptions, sea sprays and bush fires. The various industries engaged in lead-acid batteries, paint, oil refining, metal plating, phosphate fertilizer, electronic, wood production, combustion of fossil fuel, mining activity, automobile emissions, sewage wastewater, etc. releases lead in wastewater.[1] Lead toxicity causes serious dysfunction of liver, kidney, reproductive system and central nervous system, reduction in hemoglobin formation, mental retardation, infertility and abnormalities in pregnant women. Due to hazardous nature of lead (II), it directly or indirectly may cause anemia, headache, chills, diarrhea, encephalopathy, hepatitis, nephritic syndrome and even death.[2] The World Health Organization (WHO) in 1995 proposed the safe total lead limit of 50 ppb in drinking water and was decreased to 10 ppb in 2010.[3] The permissible limit of lead in drinking water as set by European Union (EU), United States Environmental Protection Agency (USEPA)[4] and Guidelines for Canadian Drinking Water Quality [5] is 10 ppb, 15 ppb and 10 ppb respectively. However, more recently an EPA document recommends a zero lead value in national primary drinking water standard.[6] Various techniques extensively used for the abatement of lead from wastewaters are chemical precipitation, membrane filtration, reverse osmosis, electrochemical reduction, ion exchange and adsorption. Among the aforementioned technologies adsorption has been preferred due to its cheapness and efficacy of heavy metal removal even in trace level. Recently bioadsorbents[7] and activated carbon obtained from agricultural by-products rich in cellulose, lignin, pectin and tannin which can serve as the adsorption sites for heavy metal ions are prominently used for wastewater treatment. The production of activated carbons from abundantly available agricultural wastes converts unwanted, additional agricultural waste to useful valuable adsorbents. The activated carbon derived from rubber tires for the removal of pesticides and chromium, [8-9] fertilizer waste [10] has been studied for the removal of contaminants from water. The adsorbents such as baggase fly ash for the treatment of wastewater containing DDD, DDE,[11] and phenol,[12] was also reported. Removal of hazardous dyes from wastewater by using bottom ash, [13-14] and carbon nanotubes[15] has been examined in the previous literature. The novel adsorbent viz. orange peels and Fe_2O_3 nanoparticles for cadmium removal,[16] Duolite C-433 for Pb (II) ions removal [17] also has been investigated as an effective adsorbents.

Chitosan, a nitrogenous polysaccharide used as cationic biosorbent obtained in enormous amount. It is a heterogeneous polymer which is composed of 2-amino-2-deoxy-D-glucopyranose and residual 2-acetamido-2-deoxy-D-glucopyranose.[18] Chitosan shows high affinity for metal ions due to the presence of amine ($–NH_2$) and hydroxyl (–OH) groups. Chitosan can bind with both anionic and cationic species. However, chitosan shows lower stability due to its hydrophilic nature and sensitivity to pH. It is soluble in most organic acids, non-porous and has a low specific surface area.[19] In order to improve chemical and mechanical strength of chitosan; several attempts of physical and chemical modification were carried out. Various chitosan based adsorbent such as bromine pretreated chitosan

RSC Advances Accepted Manuscript

composite,[20] chitosan clay composite,[21] for lead (II) ions removal has been reported. Chitosan modified by granular activated carbon for adsorption of humic acid, [22] Chitosan coated carbon for the heavy metal adsorption [23] and the activated carbon/ chitosan composite for simultaneous adsorption of aniline and Cr (VI) ion, [24] has been investigated.

The main scope of this communication is to study the modification of chitosan (CS) by doping it with activated carbon of *Luffa cylindrica* fibers (ACLF) to achieve activated carbon of *Luffa cylindrica* doped chitosan (ACLFCS) biocomposite and further to utilize it for the adsorption of lead (II) ions from water. The *Luffa cylindrica* is mainly a lignocellulosic material composed of cellulose (60%), hemicelluloses (30%) and lignin (10%) by weight[25] belongs to Cucurbitaceous family. It is abundantly available as an agricultural residue in many developing countries like India, Korea, China, Central America and Japan. Consequently these disposed, unconventional and enormously available *Luffa cylindrica* fibers can be transformed into an activated carbon which is a carbonaceous material that possesses highly developed porosity, large surface area, relatively high mechanical strength and the presence of different functional groups on its surface. The transformation of agricultural residue into an activated carbon ultimately provides a way to reduce its environmental burden or hazards. The cationic nature of CS and the anionic nature of ACLF produced a stable, granular ACLFCS biocomposite due to two opposite charged interactions. The purpose of doping of CS with ACLF is to explore the expected synergistic effects as achieved through incorporation of certain functionalities in the resultant biocomposite that are responsible for adsorption of lead (II) ions.

To the best of our knowledge, there is no literature reported on the removal of lead (II) ions from water using ACLFCS. In fact, the ability of ACLFCS to adsorb other heavy metal ions was also not reported. This gave way for more adsorption studies to be conducted using ACLFCS and to find out whether the new surface chemistry of modified chitosan have an impact on lead (II) removal from water. The present investigation aims to explore the characterization of ACLFCS using FTIR, SEM, XRD, BET analysis and accordingly used for batch adsorption of lead (II) ions from water at various parameters viz. pH, agitation time, adsorbent dosage and initial lead (II) ion concentration. The Langmuir and Freundlich isotherms were used to evaluate the equilibrium adsorption data. The adsorption rates were also determined based on the pseudo first order, Pseudo second order kinetic and intraparticle diffusion models.

2. Materials and methods

2.1 Synthesis of ACLFCS biocomposite

The *Luffa cylindrica* fruit was collected from the field of Maharashtra, India. The covering of *Luffa cylindrica* was peeled off and the exposed fibers/wood inside was washed several times with distilled water to remove dirt and dust particles. The woods were sun dried for 2 days and was cut into 1-2 cm pieces. The pieces were then oven dried at 80°C for 3-4 hours. Pyrolysis of *Luffa cylindrica* fibers was carried out in a modified muffle furnace. During pyrolysis, nitrogen at a flow rate of 100 ml/min was

RSC Advances Accepted Manuscript

used as purge gas. The furnace temperature was increased at a rate of 10ºC/min from room temperature to 700-800 ºC and was kept at this temperature for 1 hr. The sample was allowed to cool and was grounded to obtain fine powdered activated carbon. The CS (degree of deacetylation > 90 %) dissolved in 3% acetic acid heated at 40-50 °C blended with ACLF in 1:1 ratio. The mixture was stirred on magnetic stirrer at 800 rpm at room temperature for 6 hours and then dropped in 50% aqueous ammonia. Finally the mixture was filtered, washed several times with distilled water and dried in oven at 80°C. The prepared adsorbent ACLFCS was grounded to fine powder and used for the various adsorption experiments.

2.2 Characterization of ACLFCS

Characterizations of ACLFCS were carried out to understand the mechanisms of lead adsorption. Fourier transform infrared (FTIR) spectroscopy was recorded in the range of 450–4000 cm^{-1} to study the functional groups and the surface chemistry of the adsorbent using Perkin-Elmer spectrum one FTIR model, USA. The FTIR spectrum of sample was obtained by KBr pressed pellet method where a homogeneous mixture of sample with KBr in ratio of 1:50 was made. The surface morphology of synthesized biocomposite was studied by using Scanning Electron Microscope (SEM), (Zeiss Sigma, Germany) at an accelerating voltage of 15 kV. The samples were mounted on carbon tapes and supported on metallic disc. SEM photographs were taken at different magnification in the range of 20X to 5000X. X-ray diffraction (XRD) measurements were taken with Rigaku MiniFlex 2 Goniometer using Cu Kα radiation source operating under a voltage of 30 kV and a current of 15 mA. The X-ray diffraction patterns were collected with a scan rate of 5 °C/min. Brunauer–Emmet–Teller (BET) surface area of the sample and Barrett-Joyner-Halenda (BJH) pore size distribution was determined by nitrogen adsorption–desorption method at 77 K using Micromeritics ASAP 2020 V3.04 H analyzer (USA). During analysis, the sample was degassed at 100 °C in vacuum and helium was used as a carrier gas.

The elemental analysis (C/H/O/N/S) of samples (3 mg) was studied using an elemental analyzer model (Vario EL Cube) at 230V. For each analysis, the standard sulfanilic acid was first analyzed for checking the experimental error within ± 1%.

2.3 Analysis of lead (II) ions

The concentration of lead (II) ions during batch adsorption experiments was determined by using Atomic absorption spectrophotometer (SensAA GBC scientific equipment) with lead hollow cathode lamps and air acetylene mixture as an oxidant at wavelength of 283.3 nm. Deuterium background correction was used and spectral slit width was 1.3 nm. The amount of light absorbed by the test lead (II) ions solutions was compared to the amount of light absorbed by a set of standards lead (II) solutions of known concentration. A digital pH meter (Hanna instrument) was used for pH

RSC Advances Accepted Manuscript

measurement of lead (II) ion solutions. pH meter was standardized using buffer solution of pH 4 and pH 9 (Fisher Scientific, India). Rotary Shaker (Remi Make, India) at 200 rpm was used for agitating the samples during batch adsorption experiments. Three replicates were used for each adsorption experiments and average values for lead (II) ions concentration are reported.

2.4 Lead (II) ions adsorption experiments

Batch adsorption experiments were carried out to study the effect of various operating parameters viz. pH, adsorbent dosage, initial metal ion concentration and agitation time on the adsorption rate. All chemicals used were of analytical reagent grade. The standard solution of 1000 mg/L of lead (II) was prepared by dissolving lead (II) nitrate (Merck, India) and experimental solutions of the required mg/L concentration were prepared from standard lead (II) nitrate solution by successive dilutions with double distilled water. All adsorption experiments were carried out at room temperature (27±1°C) in 250 ml Erlenmeyer flasks containing 100 ml of test solution agitated on rotary shaker at 200 rpm. The effect of pH on the percentage removal of lead (II) was studied at varying pH range of 2–8 by using known volume of 35 mg/L lead (II) solutions. The required pH of the solutions was adjusted by adding 0.1 N HNO_3 or 0.1 N NaOH using digital pH meter. The specified dose of adsorbent was added to lead (II) solution and agitated at room temperature at 200 rpm for a specified period of time. The supernatant liquids obtained by filtration through Whatman filter paper-41 were analyzed for residual lead (II) ions concentration by using (AAS) Atomic absorption spectrophotometer.

For further adsorption experiments of the lead (II) solutions the optimum pH value 5 was fixed. The effect of adsorbent dosages (0.01 to 0.15 g/l) on the equilibrium adsorption of lead (II) was studied by keeping other parameters constant. Similarly the effect of varying contact time in range of 2 to 20 minutes for different lead (II) ions concentration of 35 to 115 mg/L at room temperature (27±1°C) was studied to evaluate the adsorption efficiency. The reaction mixture agitated on rotary shaker at 200 rpm and supernatant liquid was filtered and analyzed by AAS for residual lead (II) ions concentration.

The percentage removal of lead (II) was calculated using equation (1)

$$\% \text{ removal} = \frac{C_o - C_e}{C_o} x\ 100 \qquad (1)$$

Adsorption capacities were calculated using equation (2) and (3) respectively.

$$q_e = \frac{C_o - C_e}{m} x\ V \qquad (2)$$

$$q_t = \frac{C_o - C_t}{m} x\ V \qquad (3)$$

RSC Advances Accepted Manuscript

Where q_e (mg g^{-1}) and q_t (mg g^{-1}) were the amounts of lead (II) ions adsorbed at equilibrium and at time t respectively. C_o (mg L^{-1}) and C_e (mg L^{-1}) were the initial and equilibrium lead (II) ions concentration. C_t (mg L^{-1}) was the residual lead (II) ions concentration at time t. V (L) represents volume of solution and m (g) for mass of adsorbent.

3 Results and discussion

3.1 Physicochemical characterization of ACLFCS biocomposite

3.1.1. FTIR analysis

FTIR spectroscopy is used to determine the presence and absence of particular functional groups. Table 1 enlists the functional groups and Fig. 1 shows the infrared spectra of CS, ACLF and ACLFCS before and after lead (II) adsorption.

In ACLFCS biocomposite, the characteristics absorption band of CS at 2876 cm^{-1} , 1667 cm^{-1} and 1077 cm^{-1} corresponds to stretching vibration of C=O in carbonyl, NH bending vibration of NH_2 group and C-O-C stretch, was shifted to the 2883 cm^{-1} , 1696 cm^{-1} and 1071 cm^{-1} respectively. Similarly the characteristics absorption band of ACLF at 2977 cm^{-1} , 1524 cm^{-1} and 1287 cm^{-1} for aromatic C-H stretch, aromatic C=C stretch and phenolic C-O stretch shifted in ACLFCS to the wavenumber at 2993 cm^{-1}, 1531cm^{-1} and 1299 cm^{-1} respectively. FTIR study revealed the physical and chemical interaction between CS and ACLF due to which the peaks of both CS and ACLF was observed in ACLFCS biocomposite.[26] ACLFCS biocomposite also revealed the corresponding changes in characteristics absorption peaks as compared to pure CS and ACLF. The shift in absorption peaks in ACLFCS indicates the mixing and doping of ACLF with CS.

The spectral investigation of lead loaded ACLFCS showed either decrease or disappearance of peak intensity might involve in lead (II) adsorption.[27] FTIR spectrums of lead-loaded ACLFCS composite shows some shift in wavenumbers. For instance the bands at 2883 cm^{-1}, 1531 cm^{-1}, 1299 cm^{-1} , and 1071 cm^{-1} shifted to 2889 cm^{-1}, 1518 cm^{-1}, 1293 cm^{-1} and 1074 cm^{-1} respectively suggested the involvement of C=O functionalities responsible for lead (II) adsorption on ACLFCS biocomposite. Similarly the absorption bands at 3760 cm^{-1} and 1696 cm^{-1} corresponds to –OH stretching vibrations and –NH bending vibrations of $–NH_2$ group has disappeared suggested the participation of –OH and $–NH_2$ for lead (II) adsorption. Thus the FTIR study revealed the various functionalities such as C=O, –OH and $–NH_2$ liable for lead (II) adsorption on ACLFCS biocomposite.

RSC Advances Accepted Manuscript

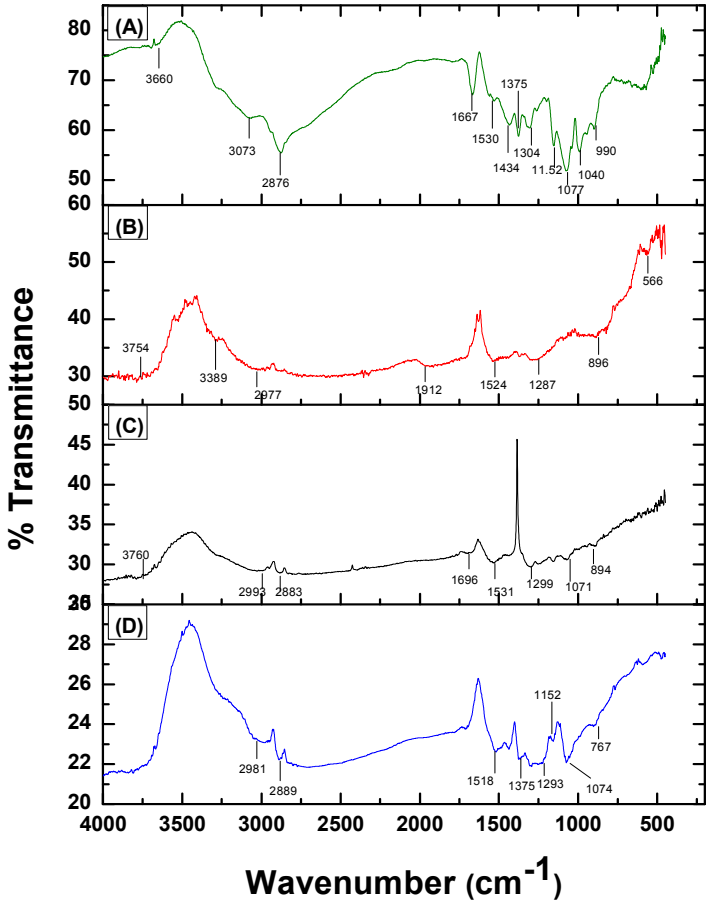

Fig. 1 FTIR of (A) CS (B) ACLF (C) ACLFCS before lead (II) adsorption and (D) ACLFCS after lead (II) adsorption.

Table 1 Surface Functional Groups of CS, ACLF and ACLFCS before and after lead (II) adsorption.

Wavenumber (cm^{-1})					
CS	ACLF	ACLFCS before adsorption	ACLFCS after adsorption	Assignment	References
3660	3754	3760	--	Hydroxyl (O-H stretch)	
3073	3389	--	--	Hydroxyl (O-H stretch)	
	2977	2993	2981	Aromatic C-H stretch	
2876	--	2883	2889	stretching vibrations of C=O in carbonyl	Xie et al.[28]
--	896	--	--	Aromatic C-H out-of-plane bending vibrations	
1667	--	1696	--	NH bending vibration of NH_2 of chitosan	Konaganti et al.[29]

RSC Advances Accepted Manuscript

1530	--	--	--	-NH bending in amide	Ramya et al.[30]
--	1524	1531	1518	Aromatic C=C stretch	Ghali et al.[31]
1262	--	--	--	Vibration of NHCO group (Amide III band)	
--	1287	1299	1293	Phenol C-O stretch	
1077	--	1071	1074	C-O-C in glycoside linkage	
990	--	--	--	Saccharide structure	
		894	767	CH_3-COH stretch	
1434	--	--	--	Bending vibration of methyl group	
1375	--	--	--	Bending vibration of methylene group	
1152	--	1158	1152	-CH vibration	
1040	--	--	--	C-O-C stretching vibration	

3.1.2 BET and elemental Analysis

N_2 adsorption–desorption isotherms and BJH based pore size distributions of CS, ACLF and ACLFCS are shown in Fig. 2 (A) and (B) respectively and detailed data of BET surface areas and PSD is represented in Table 2.

Table 2 Pore Structure Parameters of CS, ACLF and ACLFCS adsorbent.

Sorbents	BET (m^2g^{-1})	V_{total} (cm^3g^{-1})	V_{micro} (cm^3g^{-1})	V_{meso} (cm^3g^{-1})	Mean pore diameter (Å)
CS	3.5	4.582 x 10^{-3}	4 x10^{-3}	5.82 x 10^{-4}	52.36
ACLF	285	0.2076	0.1861	0.0215	29.13
ACLFCS	138	0.1117	0.0989	0.0128	32.37

Where V_{total}: total pore volume, V_{micro}: micropore volume, V_{meso}: mesopore volume of CS, ACLF and ACLFCS.

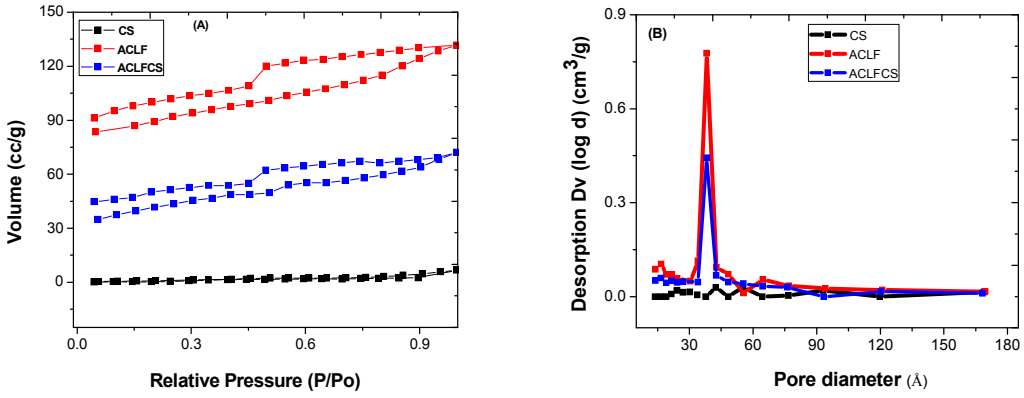

Fig. 2 (A) Nitrogen adsorption v desorption isotherm (B) BJH based pore size distribution of CS, ACLF and ACLFCS biocomposite.

RSC Advances Accepted Manuscript

The surface area of synthesized ACLFCS adsorbent was higher with respect to pure CS and lower with respect to ACLF. The decreased surface area of ACLFCS may be due to the blockage of internal porosity of ACLF by CS and successful blending between them. The surface area of the adsorbent is one of the physical parameter for adsorption phenomenon. The adsorptive capacity of adsorbent increases with increasing surface area for pure physisorption process. In present study the physisorption of ACLFCS for lead (II) ions removal is limited and mainly the chemisorption mechanism occurred. In ACLFCS biocomposite even though the surface area decreased but it incorporated the functional groups like $–NH_2$, -OH and C=O that were responsible for lead (II) adsorption. These related functionalities are cleared from FTIR study.

The N_2 adsorption-desorption isotherms for CS is of type II according to IUPAC classification with a very narrow hysteresis loop indicative of mesoporous materials. In contrast, ACLF demonstrate typical Type IV isotherm and displays a broad H_2 hysteresis loop in the range of 0.4–1.0 P/Po which is a characteristics of ordered mesoporous materials. The ACLFCS biocomposite has a combined isotherm of two individual components viz. CS and ACLF along with intermediate value of specific surface area and pore volume to that of CS and ACLF. In ACLFCS there is a hysteresis loop at a relative pressure above 0.4, indicative of mesoporosity. The appearance of the intermediate mesoporosity in the biocomposite may arise from interspaces between CS and ACLF with different framework structures. The average pore diameter values (pore diameter > 2 nm) as shown in table 2, corresponds to the presence of mesoporous structure for all CS, ACLF and ACLFCS adsorbents. Due to good BET surface area, the prepared biocomposite is reasonably worthy for lead (II) adsorption.

Table 3 Proximate and Ultimate analysis of ACLFCS adsorbent.

	Ultimate analysis (%)					Proximate analysis (%)			
Sorbent	C	H	N	S	O	Moisture	Volatile matter	Ash	Fixed Carbon
ACLFCS	50.94	5.14	1.57	0.29	42.06	8.92	47.78	4.3	39

The burnt carbonaceous portion leaves the residue called ash which is not required and considered as an impurity in activated carbon. As the ash content is low and found to be 4.3% which is in range of most ash content of agricultural waste. The prepared biocomposite resembles a good adsorbent. The density of carbonaceous adsorbent plays a vital role in adsorption. The carbon with higher bulk density will be more efficient in removal of contaminants. According to Itodo et al., (2008) bulk density has impact on adsorbate-retention level by any adsorbent.[32] The higher density carbons hold more adsorbate per unit volume. It is verified that there is a linear relationship between porosity and bulk density prior to the adsorption. Higher porosity carbon was apparently denser. It is the porosity that capitulate the surface areas for the adsorbate to adsorb. In this research work the average bulk density of ACLFCS was found 0.69 g ml^{-1}.

RSC Advances Accepted Manuscript

3.1.3. SEM analysis

In order to confirm the adsorption of lead (II) ions onto ACLFCS biocomposite and for better insight regarding the alteration of the surface morphology after metal ions adsorption, a microscopic SEM analysis was applied. The SEM image of pure CS is shown in Fig. 3(A). The SEM images of ACLFCS before lead (II) adsorption are shown in Fig. 3 (B) and (C) while ACLFCS after lead (II) adsorption are represented in Fig. 3 (D) and (E). The surface morphology of CS appeared to possess uneven texture, bumpiness and porous cavities. ACLFCS before lead (II) adsorption as in Fig. 3 (B-C) possesses porous texture with round and elliptical shaped voids that can provide the adsorption sites to the adsorbate and consequently represents different surface morphology than with pure CS. The surface morphology of ACLFCS after lead (II) adsorption as depicted in Fig. 3 (D) shows the accumulation of new shiny white clumps on the adsorbent surface similarly Fig. 3 (E) revealed the appearance of reduced pore size due to the coverage of smooth, whitish layer on the adsorbent. The SEM images of lead (II) loaded adsorbent found to be exhausted which was not seen before metal loading. It followed that the adsorbent cavities occupied / filled by lead (II) ions after adsorption.

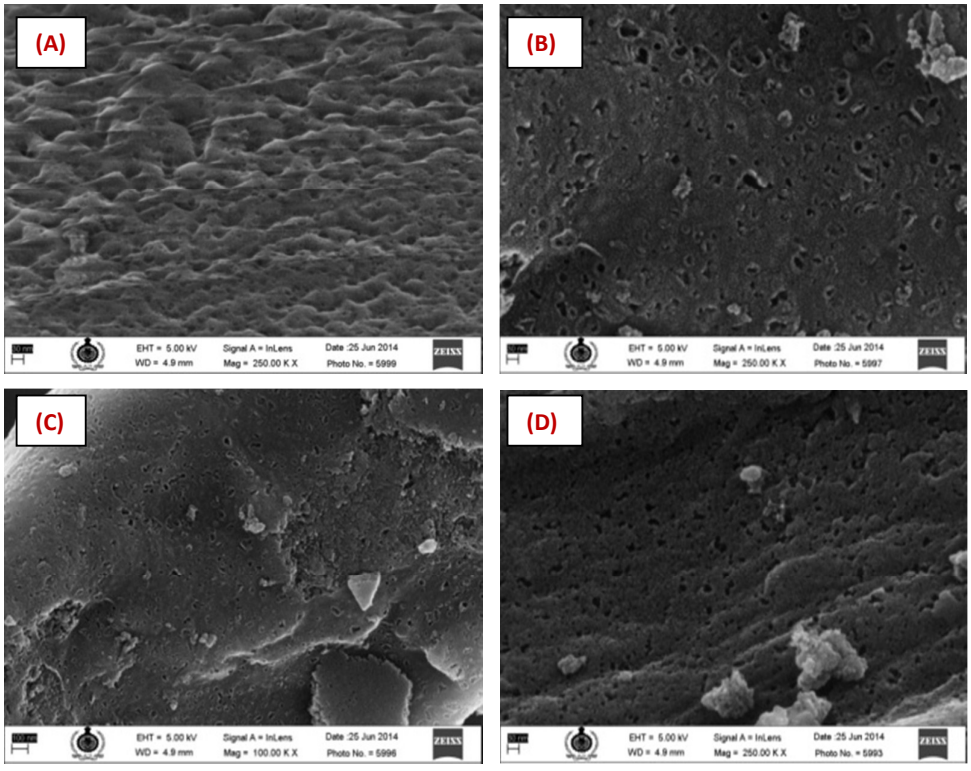

RSC Advances Accepted Manuscript

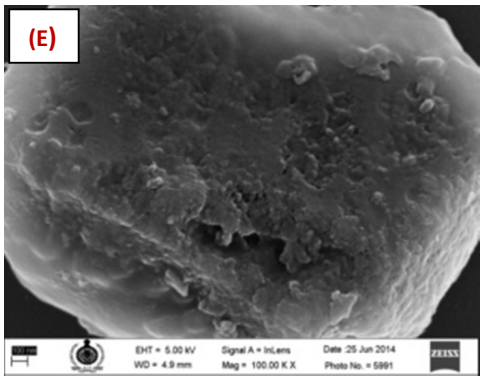

Fig. 3 SEM characterization of (A) CS at 250 X (B) ACLFCS before lead (II) adsorption at 250 X and (C) at 100 X (D) ACLFCS after lead (II) adsorption at 250 X and (E) at 100 X.

3.1.4. XRD

XRD pattern of pure CS, ACLF and ACLFCS biocomposite before and after lead (II) adsorption, are shown in Fig. 4 (A-D). X ray diffraction pattern of CS as shown in Fig.4(A) exhibited broad diffraction peak at 2θ = 20° with d- spacing of 4.2 Å is characteristics of semi crystalline chitosan. The peaks are broadened due to the amorphous nature of CS polymer. Several researchers reported activated carbon as an amorphous carbon.[33-35] The prepared ACLF as depicted in Fig. 4 (B) shows amorphous structure. There are two broad peaks observed near 2θ = 24° and 42° that are common in activated carbon and are assigned to (002) and (10) reflections. In ACLFCS biocomposite before lead (II) adsorption as shown in Fig. 4 (C), the XRD pattern shows both the peaks at 2θ = 19.28° corresponding to CS and a small hump at 2θ = 42° a characteristics of ACLF which was completely absent in pure CS. The above result shows that the doping and incorporation of ACLF with CS was effective to achieve ACLFCS biosorbent. The XRD pattern of lead loaded adsorbent Fig. 4 (D) identified lead minerals on the surface of ACLFCS as hydrocerrusite – $Pb_3(CO_3)_2(OH)_2$. The precipitation of hydrocerrucite on ACLFCS might be attributed to the contribution of specific surface functional groups.[36] The XRD pattern of lead loaded adsorbent was identified by JCPDS file no. 13-0131. XRD analysis of lead adsorbed ACLFCS shown typical peaks at 2θ = 19.94°, 19.98°, 24.76°, 27.22°, 34.18°, 35.94°, 40.48°, 42.36°, 44.02°, 49.02°, 53.96°, 57.9° and 75.76° corresponds to (101), (012), (104), (015), (110), (113), (202), (024), (205), (119), (122), (114) and (312) Bragg reflections respectively. Thus the presence of lead peaks in lead loaded ACLFCS shows the adsorption of lead (II) ions on the adsorbent surface.

RSC Advances Accepted Manuscript

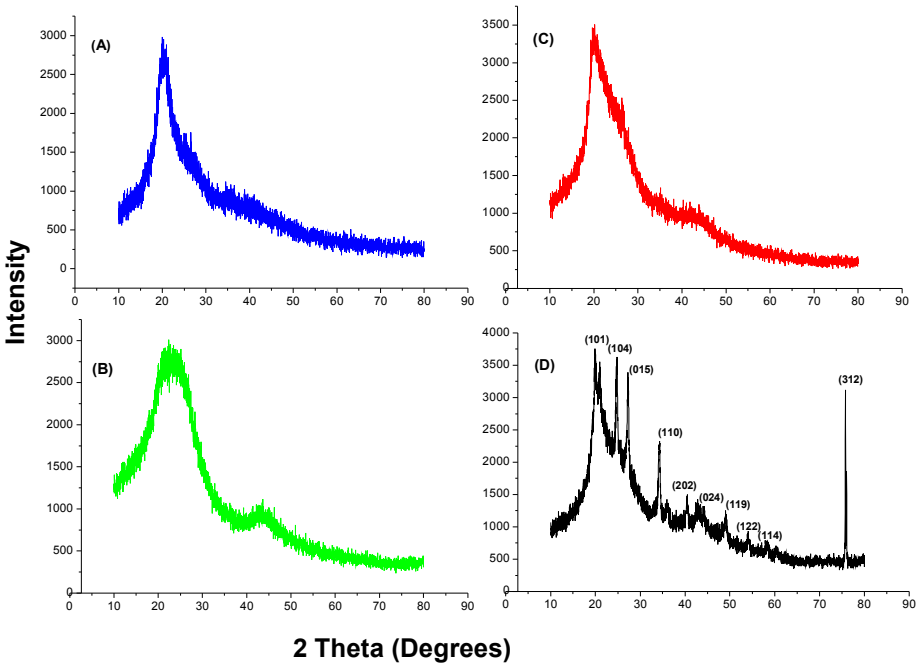

Fig. 4 XRD of (A) CS (B) ACLF (C) ACLFCS before lead (II) adsorption and (D) ACLFCS after lead (II) adsorption.

3.2 Effect of pH

The pH of solution is most essential factor affecting solution chemistry, chemical speciation of metal ion and degree of ionization of functional groups on the adsorbent surface. The chemical reactions such as hydrolysis, complexation, redox and precipitation are intensely influenced by pH.[37] The effect of pH on lead (II) adsorption is shown in Fig. 5. The results showed that the percentage uptake of lead (II) increased significantly as the pH increased from 2 to 5 and attains equilibrium up to pH 6 whereas the decreased lead (II) adsorption is observed at increased pH range of 6-8. Similarly adsorption negatively correlated with acidic medium. The main species of lead (II) is Pb^{2+} under weakly acidic condition i.e at pH < 6. At pH 6, Pb^{2+} and Pb $(OH)^{+}$ are in equal concentration. At increasing alkaline conditions viz. pH range of 7-9 lead forms lead hydroxides such as Pb $(OH)^{+}$ that eventually precipitates as Pb $(OH)_2$ at pH > 9 and Pb $(OH)_3^{-}$ at pH > 11. At lower pH value i.e. at pH < 5, the adsorption was repressed possibly as a result of increased H_3O^{+} ion concentration that competes with positively charged metal ion for the adsorption sites on adsorbent. Accordingly, the adsorption of lead (II) on ACLFCS at pH < 5 could be resulted from the cation exchange reactions. As the pH increased, i.e at pH 5 to 6, the high adsorption of lead (II) occurs which can be attributed to the increased negative charge density on the adsorbent that weakens the competition between H_3O^{+} and lead (II) ions for the adsorbent surface. Thus the improved adsorption of lead (II) ions at pH 5-6 governs by the electrostatic interaction. The declined adsorption amount at higher pH (>6) is probably due to the metal hydrolysis and precipitation of lead (II) as lead hydroxides. Therefore the adsorption process is a combination of ion exchange and precipitation. In this research work, the

RSC Advances Accepted Manuscript

optimum pH 5 was recorded for lead (II) removal and hence the further adsorption experiments were carried out at this pH value. The region where there is a sharp increase in adsorption capacity from low to high pH can be called pH adsorption edge.[38] In this study, the pH adsorption edge was 2–5. (**Fig. 5** Effect of pH on lead (II) adsorption, please see electronic supplementary information ESI 1).

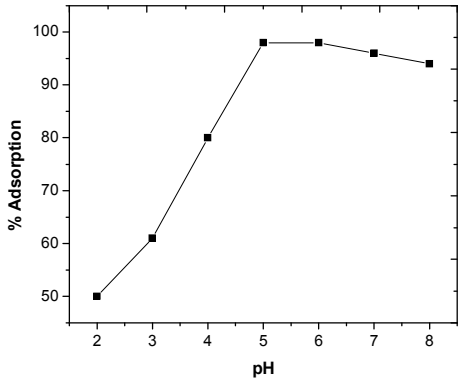

Fig. 5 Effect of pH on lead (II) adsorption.

3.3 Effect of dose of adsorbent

The effect of adsorbent dosage at room temperature (27 ± 1°C) on lead (II) adsorption is shown in Fig. 6. The result showed that the percentage removal of lead (II) increases with increase in adsorbent dosage (0.01– 0.1 g/l) with adsorption capacity of 81 to 98 % at optimum pH 5. It was observed that lead (II) uptake was rapidly increased with increasing adsorbent dosage from 0.01 to 0.1 g/L and further no substantial uptake of lead (II) ions occurred at further increased dose of adsorbent. This fact is expected because as the adsorbent doses increases, the number of adsorbent particles and consequently the adsorption sites on the adsorbent surface increases, allowing the easier penetration of lead (II) ions. The further increase of adsorbent doses has no significant effect on the percentage lead (II) removal as system reaches the equilibrium. The maximum adsorption occurred at dosage of 0.1 g/L. Thus optimum adsorbent dosage of 0.1 g/L is justified for economical purposes.

(**Fig. 6** Effect of adsorbent doses on lead (II) adsorption, please see electronic supplementary information ESI 2)

RSC Advances Accepted Manuscript

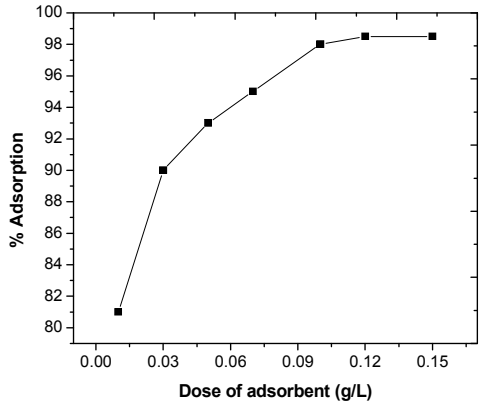

Fig. 6 Effect of adsorbent doses on lead (II) adsorption.

3.4 Effect of Contact time on different lead (II) ions concentration

Adsorption of lead (II) ions as a function of contact time on varying lead (II) ions concentration from 35 mg/L to 115 mg/L at optimum pH 5 is shown in Fig. 7. The plot showed that the rate of lead (II) ions adsorption consisted of two phases; an initial rapid phase and a second slower equilibrium phase of adsorption. The result indicated that the uptake of lead (II) ions increases with time from 2 to 15 minutes with maximum 98 % (for 35 mg/L) to 86 % (for 115 mg/L) lead (II) removal efficiency and thereafter, the rate of adsorption become slower near the equilibrium. It is found that the time required to attain equilibrium is relatively short as compared to others reported in the literature.[39] The results confirmed that with a fixed dose of adsorbent at increasing lead (II) ion concentration, the amount adsorbed increased but the adsorption percentage decreased. Initially, the fast removal of lead (II) ions is obvious as large numbers of unoccupied adsorbent surface sites are available for the adsorption. By the progress of time equilibrium adsorption achieved may be due to the accumulation of lead (II) ions on the vacant sites caused limited mass transfer of the adsorbate from the bulk liquid to the external surface of the adsorbent.[21] From Fig. (7) it is also evident that the percentage removal of lead (II) decreases with increase in initial lead (II) ions concentration. It can be explained by the fact that, at high lead (II) ions concentration, the available apparent external adsorbent sites are already occupied which prevents the diffusion of lead (II) ions on adsorbent surface.

RSC Advances Accepted Manuscript

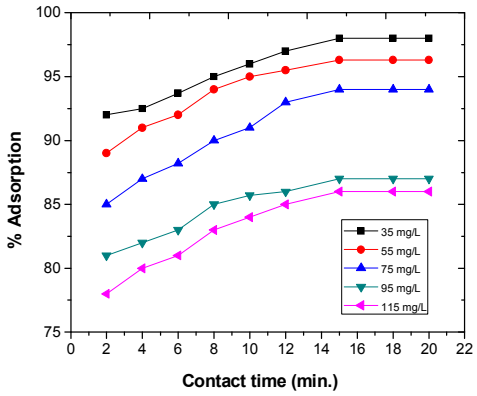

Fig. 7 Effect of contact time on lead (II) ions adsorption at different initial concentrations.

3.5 Regeneration studies

The percentage desorption of lead (II) ions is depicted in Fig. 8. In present work, five adsorption-desorption cycles were carried out with 35 mg/L lead (II) ions concentration. 0.01 g of lead loaded ACLFCS adsorbent was washed with distilled water, air dried and placed in contact with 0.1M HCl as desorption agent in 250 ml Erlenmeyer flasks. Desorption experiments were carried out at pH < 3. The flasks were agitated at 200 rpm at 27 °C for 1 hr. to ensure the equilibrium. 0.1 M HCl found to be better desorbing agent at pH 2 due to high amount of H^+ ions in the solution. This results in exchange of ions where H^+ takes the place of lead (II) ions in solution. To estimate the process of lead (II) desorption, the lead (II) ions concentration present in 0.1 M HCl were analyzed using Atomic absorption spectrophotometer. The percentage desorption of lead (II) was calculated using equation (4).

$$\% \text{ desorption} = \frac{C_{Ads} - C_{Des}}{C_{Ads}} \text{ X } 100 \qquad (4)$$

Where C_{Ads} and C_{Des} are the concentration of lead (II) ions adsorbed and desorbed (mg L^{-1}) respectively. The results shows that the percentage recoveries of metal ions decreased by 28 % at the end of fifth adsorption desorption cycle due to saturation of adsorbent binding sites.

RSC Advances Accepted Manuscript

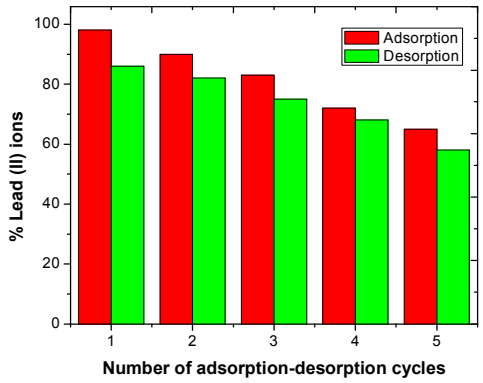

Fig. 8 Adsorption-Desorption cycles of lead (II) ions concentration using ACLFCS biocomposite.

3.6 Adsorption kinetics

To study the mechanism and kinetics of lead adsorption, characteristics adsorption constants were determined using pseudo first order, pseudo second order and an intraparticle diffusion models. A rate equation for the pseudo first order[40] is generally expressed as follows:

$$\text{Log}\,(q_e\text{-}q_t) = \text{Log}\,q_e - \frac{K_1}{2.303}\,t \qquad (5)$$

Where q_e and q_t are the sorption capacities at equilibrium and at time t respectively (mg g^{-1}) and K_1 is the rate constant of pseudo first order sorption (min^{-1}). Fig. 9 (a) shows the Lagergren pseudo first order kinetic plot for the adsorption of lead (II) ions onto ACLFCS. The pseudo first order rate constant can be obtained from the slope of plot of Log ($q_e - q_t$) against time; t. The kinetic parameters were summarized in Table 4. From Lagergren's model the lower linear correlation coefficient (R^2) and much higher calculated q_e value than observed experimental value does not represent a good fit with the adsorption experimental data.

Ho presented a pseudo second order rate law expression, which demonstrated how the rate depended on the adsorption equilibrium capacity but not the concentration of the adsorbate.[41] The integrated linear form of pseudo second order rate expression is as follows:

$$\frac{t}{q_t} = \frac{1}{K_2 {q_e}^2} + \frac{t}{q_e} \qquad (6)$$

Where t is the contact time (min), q_e (mg g^{-1}) and q_t (mg g^{-1}) are the amounts of solute adsorbed at equilibrium and at any time, t respectively. Fig. 9 (b) shows the pseudo second order kinetic plot for adsorption of lead (II) ions onto ACLFCS. Equilibrium adsorption capacity (q_e) and the pseudo second order rate constants K_2 were obtained from the slope and intercept of the plots of t/q_t against t. The calculated parameters are given in Table 4. The Results presented in table clearly shows that the coefficient of determination for pseudo second order equation (R^2= 0.99) is higher than pseudo first

RSC Advances Accepted Manuscript

order. Similarly calculated q_e value from pseudo second order is closer and in good agreement with the experimental value suggested that the adsorption phenomenon of lead (II) by ACLFCS follows the pseudo second order kinetics. This indicated that the rate determining step of this adsorption system may be chemisorptions involving valence forces through sharing or exchange of electrons between adsorbent and adsorbate.[42]

The intraparticle diffusion model developed by Weber and Morris, McKay and Poots**.** The linear form of equation for intra-particle diffusion is as follows:

$$q_t = K_i t^{0.5} + C \qquad (7)$$

where q_t is the amount of adsorbate adsorbed on the surface of the adsorbent at that particular time t (mg g^{-1}), t is the time of adsorption (min), k_i is the intra-particle diffusion rate constant (mg g^{-1} $min^{-0.5}$) and C is the intercept which represents the value of the thickness of the boundary layer.[43] The intraparticle diffusion plot of q_t versus square root of time ($t^{0.5}$) is shown in Fig. 9 (c). From figure, it is followed that the intraparticle diffusion plot is not linear over the whole range of time; however it exhibits multi linearity revealing the existence of different adsorption stages of mass transport. The multi linearity can be attributed to the faster mass transfer through the boundary layer diffusion, intra-particle diffusion state which is highly involved in rate control of this mechanism and final slow equilibrium stage. According to this model, the plot should be linear and if these lines pass through the origin then intraparticle diffusion is the rate-limiting step.[44] When the plots do not pass through the origin, it indicates some degree of boundary layer control and further shows that the intra-particle diffusion is not the only rate-limiting step but also other kinetic models may control the rate of adsorption, all of which may be operating simultaneously. The intraparticle diffusion K_i value was obtained from the slope of plot of q_t versus $t^{0.5}$. The correlation coefficients (R^2 = 0.90) for the intraparticle diffusion model at (27 ± 1°C) and it was observed that the straight line does not pass through the origin indicates that the intraparticle diffusion was the part of adsorption but not the only rate-controlling step.

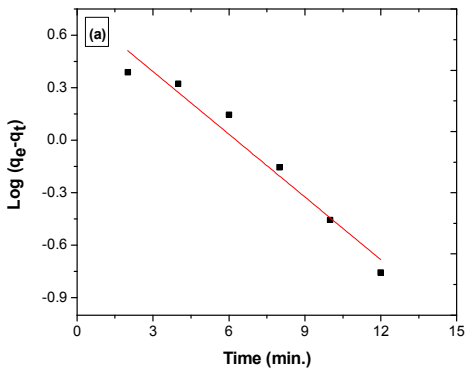

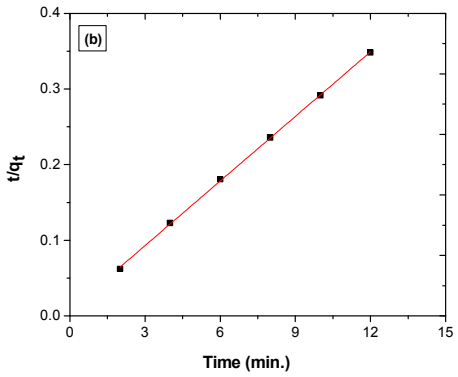

RSC Advances Accepted Manuscript

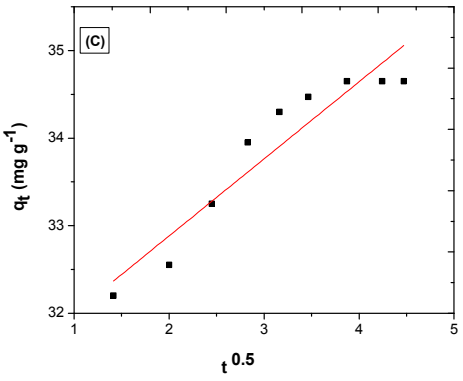

Fig. 9 (a) Plot of pseudo first order kinetic (b) Plot of pseudo second order kinetic (c) Plot of intraparticle diffusion model.

Table 4 Pseudo first order, pseudo second order and intraparticle diffusion rate constants for lead (II) ions onto ACLFCS.

Metal	Pseudo - first-order				Pseudo-second-order			Intraparticle diffusion model		
Lead (II)	K_1 (min^{-1})	q_e (mg g^{-1})	R^2	q_e (cal.)	K_2 (g $mg^{-1}min^{-1}$)	q_e (mg g^{-1})	R^2	$K_i t$ (mg g^{-1} $min^{-0.5}$)	C (mg g^{-1})	R^2
Value	-0.27	5.636	0.96	34.65	0.11	35.71	0.99	0.88	31.12	0.90

3.7 Adsorption isotherm

Adsorption isotherm represents the relationship between the amounts of adsorbate adsorbed per unit mass of adsorbent and the concentration of adsorbate in the equilibrium solution at a given temperature. Adsorption isotherm provides information on adsorption mechanisms, surface properties and affinity of an adsorbent towards heavy metal ions. The mechanism of adsorption of lead (II) by ACLFCS was studied by fitting the experimental data to most widely used Langmuir and Freundlich adsorption isotherms.

Freundlich isotherm is an empirical equation used to describe multilayer adsorption (heterogeneous system).[45] The linear form of Freundlich isotherm is expressed as below:

$$\ln q_e = \ln K_f + \frac{1}{n} \ln C_e \qquad (8)$$

Where K_f and n are the Freundlich isotherm constants indicating adsorption capacity and adsorption intensity respectively. q_e (mg g^{-1}) is the observed lead (II) adsorption capacities and C_e (mg L^{-1}) is the equilibrium concentration. The Freundlich plots of log C_e against log q_e gives a straight line of slope 1/n and intercept K_f as shown in Fig. 10 (a). The Freundlich adsorption parameters i.e.

RSC Advances Accepted Manuscript

maximum adsorption capacities (K_f), adsorption intensity (n) and correlation coefficient (R^2) are given in Table 5. The values of K_f and 1/n were found to be 41.39 mg/g and 0.29 respectively. Since the value of 1/n is less than 1, it indicates a favorable adsorption but the low correlation coefficient R^2 = 0.95 indicates no better fit and applicability of Freudlich model for the adsorption of lead (II) ions on ACLFCS.

The Langmuir model assumes that the monolayer adsorption occurs at finite numbers of homogeneous sites on the adsorbent.[46] It is also noteworthy that the shape of the isotherm obtained from Langmuir plot can provide some information on adsorbate-adsorbent interaction. The linear form of Langmuir equation can be expressed as follows:

$$\frac{C_e}{q_e} = \frac{1}{q_m b} + \frac{C_e}{q_m} \qquad (9)$$

Where q_e (mg g^{-1}) and q_m (mg g^{-1}) are the observed and maximum lead (II) adsorption capacities, C_e (mg L^{-1}) is the equilibrium concentration of lead (II) in solution and b (L mg^{-1}) is the equilibrium constant related to energy of adsorption. The Langmuir plot of C_e against C_e/q_e is shown in Fig. 10 (b). The values of q_m and b are obtained from the slope $1/q_m$ and intercept $1/(q_m b)$ of the plot of C_e/q_e against C_e. The Langmuir parameters R^2, b and q_m are shown in Table 5. The Langmuir isotherm model also provides a dimensionless constant separation factor R_L expressed as $R_L = 1/(1 + b.C_o)$. [47] Where b is the Langmuir constant and C_o is the highest initial lead (II) ion concentration (mg L^{-1}). From Fig.10 (b) the maximum adsorption capacity (q_m) and Langmuir constant (b) were found to be 112 mg g^{-1} and 0.50 L mg^{-1} respectively. The correlation coefficient R^2 = 0.98 was closer to unity, shows that the adsorption data better fitted to the Langmuir plot. The value of R_L for 35 mg L^{-1} to 115 mg L^{-1} lead (II) ion concentration was in the range of 0.0540-0.0170 and this specifies the favorable adsorption onto ACLFCS under the optimized experimental conditions. Further the plot of C_e versus q_e as shown in Fig. 10 (c) obtained is "H" type isotherm in Giles classification system.[48] The H-type isotherm usually indicates chemical adsorption (chemisorptions) and reflects a relatively high affinity or strong interaction between adsorbate and the adsorbent.

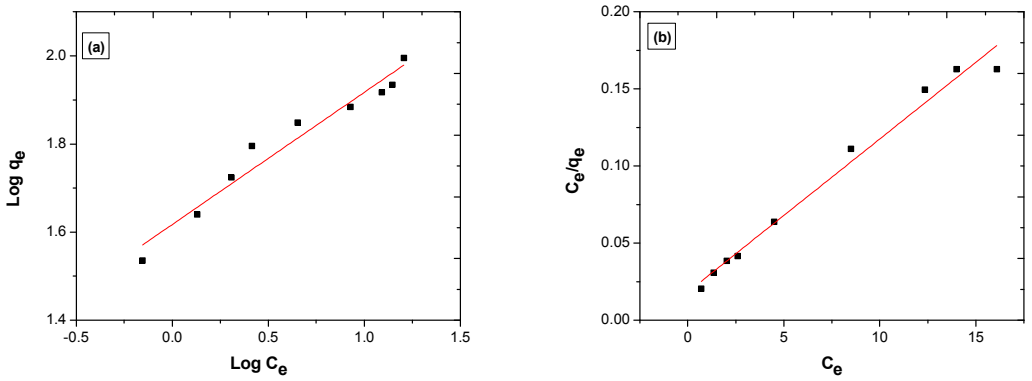

RSC Advances Accepted Manuscript

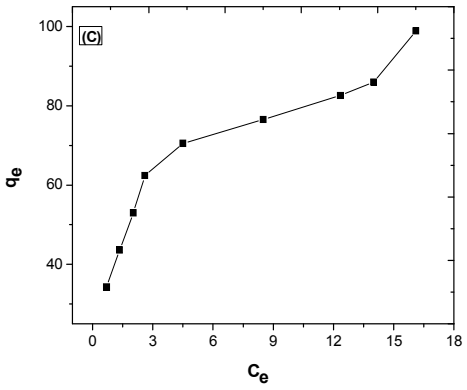

Fig. 10 a) Freundlich adsorption isotherm plot b) Langmuir adsorption isotherm plot c) Plot of C_e Vs. q_e.

Table 5 Langmuir and Freundlich parameters for the adsorption of lead (II) ions on ACLFCS.

Equilibrium model	Langmuir constants				Freundlich constants		
Parameters	q_m (mg g^{-1})	b (L mg^{-1})	R^2	R_L	K_f (mg g^{-1})	1/n	R^2
Values	112	0.50	0.98	0.0540-0.0170	41.39	0.29	0.95

The comparative equilibrium adsorption capacity of lead (II) ions on previously reported adsorbents is given in Table 6. ACLFCS has a much higher value of adsorption capacity compared to other adsorbents. The results revealed ACLFCS as promising adsorbent for mitigation of lead (II) from aqueous solution.

Table 6 Adsorption capacities of lead (II) ions by various adsorbents.

Adsorbent	**q_m (mg g^{-1})**	**pH**	**References**
Bromine pretreated chitosan	1·755	5-5.5	Dongre et al.[20]
Cross linked chitosan clay beads	7.93	4.5	Tirtom et al. [21]
Epichlorohydrin cross linked chitosan beads	39.42	6	Gyananath and Balhal[49]
Chitosan	47.393	6	Asandei et al. [50]
Activated carbon of coffee residue	63	5.8	Boudrahema et al. [51]
Iodate doped chitosan composite	22.22	6	Gedam and Dongre [52]
Nano silversol-coated activated carbon	23.81	5.5	Senthil kumar et al. [53]
Activated carbon of *Spartina alterniflora*	99	4.8-5.6	Li and Wang. [4]
Date stone activated carbon	19.64	6	Mounia et al. [54]
Heartwood charcoal of Areca catechu	2.198	5	Haloi et al. [55]
Tamarind wood activated carbon	43.85	5.6	Acharya et al. [56]

RSC Advances Accepted Manuscript

Luffa cylindrica fibers	4.63	4	Saueprasearsit et al. [57]
NaoH modified *Luffa cylindrica* fibers	13.48	4	Saueprasearsit et al. [57]
Luffa charcoal	51.02	5	Umpunch et al. [58]
ACLFCS	112	5	This study

Conclusion

The present investigation shows that ACLFCS is an effective adsorbent for the mitigation of lead (II) ions from aqueous solution. The removal of lead (II) using ACLFCS biocomposite was pH dependent and maximum 98-99% lead (II) removal occurred at pH 5 in contact time of 15 minutes at an optimum dose of 0.1 g/L suggested reasonable and cost-effective adsorption technique. The adsorption experimental data were fitted to Langmuir and Freundlich isotherm models. Experimental results are in good agreement with Langmuir adsorption isotherm model with maximum monolayer adsorption capacity of 112 mg/g. The kinetic study demonstrates that sorption process obeyed pseudo second order kinetic model suggested that both adsorbate and adsorbent are involved in rate-determining step. The FTIR study revealed the functional groups –OH, -NH_2 and C=O were mainly concerned with the adsorption of lead (II) ions onto ACLFCS. The BET surface area of ACLFCS after modification decreases signifies that the physisorption of lead (II) ions is limited and the adsorptive mechanisms will mainly be the chemisorptions. The cost of lead (II) removal using ACLFCS is expected to be quiet low as the raw materials of synthesized adsorbent are easily available in large amount conveys us the new consideration for the increasing pressure of worldwide environmental pollution.

Acknowledgements

The authors are thankful to the Director, VNIT Nagpur (India) and DIAT Pune (India) for technical assistance in characterization of the samples. Thanks are also given to Dr. Bansiwal, Sr. Scientist NEERI for providing XRD analysis.

References

1. C. K. Singh, J. N. Sahu, K. K. Mahalik, C.R. Mohanty, B. Raj Mohan and B.C. Meikap, Studies on the removal of Pb (II) from wastewater by activated carbon developed from Tamarind wood activated with sulphuric acid, *Journal of Hazardous Mater*., 2008, **153**, 221–228.
2. B. L. Martins, C.C.V. Cruz, A. S. Luna and C.A. Henriques, Sorption and desorption of Pb^{2+} ions by dead *Sargassum* sp. biomass, *Biochemical Engineering J.,* 2006, **27**, 310- 314.
3. WHO Guidelines for Drinking-water Quality, 4th ed., WHO Press, Geneva, 2011, http://www.who.int.

RSC Advances Accepted Manuscript

4. K. Li and X. Wang, Adsorptive removal of Pb (II) by activated carbon prepared from *Spartina alterniflora:* equilibrium, kinetics and thermodynamics, *Bioresource Technol*., 2009, **100,** 2810–2815.
5. Guidelines for Canadian Drinking Water Quality, 2012 www.healthcanada.gc.ca/waterquality
6. Current Drinking Water Standards, EPA, office of Water, 2002. http://www.epa.gov/safewater/mcl
7. V.K. Gupta, A. Nayak and S. Agarwal, Bioadsorbents for remediation of heavy metals: Current status and their future prospects, *Environ. Engg. Res*., 2015, 20, 1-18.
8. V.K. Gupta, B. Gupta, A. Rastogi, S. Agarwal and A. Nayak, Pesticides removal from waste water by activated carbon prepared from waste rubber tire, *Water research*, 2011, **45**, 4047-4055.
9. V.K. Gupta, I. Ali, T.A. Saleh, M.N. Siddhiqui and S. Agarwal, Chromium removal from water by activated carbon developed from waste rubber tires, *Envi. sci pollution research*, 2013, **20**, 1261-1268.
10. V.K. Gupta, S.K. Srivastava, D. Mohan and S. Sharma, Design parameters for fixed bed reactors of activated carbon developed from fertilizer waste for the removal of some heavy metal ions, *Waste Management*, 1998, **17**, 517-522.
11. V.K. Gupta and I. Ali, Removal of DDD and DDE from wastewater using bagasse fly ash- a sugar industry waste, *Water research*, 2001, **35**, 33-40.
12. V. K. Gupta, S. Sharma, I. S. Yadav and D. Mohan , Utilization of bagasse fly ash generated in the sugar industry for the removal and recovery of phenol and *p* - nitrophenol from wastewater, *J. Chem. Tech. Biotech*., 1998, **71**, 180-186.
13. V.K. Gupta, A. Mittal, D. Jhare and J. Mittal, Batch and bulk removal of hazardous coloring agent Rose Bengal by adsorption techniques using bottom ash as adsorbent, *RSC advances*, 2012,**2**, 8381-8389.
14. V.K. Gupta, I. Ali, V.K. Saini, T.V. Gerven, B.V. Bruggen and C. Vandecasteele, Removal of dyes from wastewater using bottom ash, Ind. Engg. Chem. Res., 2005, 44, 3655-3664.
15. V.K. Gupta, R. Kumar, A. Nayak, T.A. Saleh and M.A. Barakat, Adsorptive removal of dyes from aqueous solution onto carbon nanotubes: A review, *Advances in Colloid and Interface Sci*., 2013, **193-194**, 24-34.
16. V.K. Gupta and A. Nayak, Cadmium removal and recovery from aqueous solutions by novel adsorbents prepared from orange peel and Fe_2O_3nanoparticles, *Chem. Eng. J*., 2012, **180**, 81-90.
17. V.K. Gupta, P. Singh and N. Rahman, Adsorption behavior of Hg (II), Pb (II), and Cd (II) from aqueous solution on Duolite C-433: a synthetic resin, *J. of colloid interface science*, 2004, **275**, 398-402.

RSC Advances Accepted Manuscript

18. M. Rinaudo, Chitin and chitosan: Properties and applications, *Prog. Polym. Sci.,* 2006, **31**, 603-632.
19. G. Crini, Recent developments in polysaccharide-based materials used as adsorbents in wastewater treatment, *Prog. Polym. Sci*., 2005, **30**, 38-70.
20. R. S. Dongre, M. Thakur, D. Ghugal and J. Meshram, Bromine pretreated chitosan for adsorption of lead (II) from water, *Bull. Mater. Sci*., 2012, **35**, 875-884.
21. V. N. Tirtom, A. Dincer, S. Becerik, T. Aydemir and A. Celik, Removal of lead (II) ions from aqueous solution by using cross linked chitosan clay beads, *Desalination and water treatment,* 2012*,* **39**, 76-82.
22. S. Maghsoodloo, B. Noroozi, A. K. Haghi and G. A. Sorial, Consequence of chitosan treating on the adsorption of humic acid by granular activated carbon, *J. Hazard. Mater*., 2011, **191**, 380-387.
23. M. Soundarrajan, T. Gomathi and P. N. Sudha, Understanding the adsorption efficiency of chitosan coated carbon on heavy metal removal, *Int. J. of Sci. & Res. Publ*., 2013, **3**, 1-10.
24. R. Huang, B. Yang, Q. Liu and Y. Liu, Simultaneous Adsorption of Aniline and Cr(VI) Ion by Activated Carbon/ Chitosan Composite, *J. Appl. Polym.Sci*., 2014, **131**, 1-9.
25. I. O. Mazali and O. L. Alves, Morphosynthesis: high fidelity inorganic replica of the fibrous network of loofa sponge (*Luffa cylindrical)*, *Anais da Academia Brasileira de Ciencias,* 2005, **77**, 25-31.
26. Y. J. Yin, K. D. Yao, G. X. Cheng and J. B. Ma, Properties of polyelectrolyte complex films of chitosan and gelatin*, Polymer International,* 1999, **48**, 429-432.
27. Y. Nuhoglu and E. Malkov, Thermodynamic and kinetic studies for environmentally friendly Ni(II) biosorption using waste pomace of olive oil factory, *Bioresource Technol*., 2009, **100**, 2375-2380.
28. Y. Xie, S. Li, F. Wang and G. Liu, Removal of perchlorate from aqueous solution using protonated crosslinked chitosan, *Chem. Eng. J*., 2010, **156**, 56-63.
29. V.K. Konaganti, R. Kotaa, S. Patil and G. Madras, Adsorption of anionic dyes on chitosan grafted poly (alkyl methacrylate), *Chem. Eng. J*., 2010, **158**, 393-401.
30. R. Ramya, P.N. Sudha and J. Mahalakshmi, Preparation and characterization of Chitosan binary blend, *Int. J. of Sci. and Res. Publication,* 2012, **2**, 1-9.
31. A. E. Ghali, I. B. Marzoung, M. H. V. Baouab and M. S. Roudesli, Separation and characterization of new cellulosic fibers from Jancus acutus plant, *Bioresources,* 2012, **7**, 2002-2018.
32. A. U. Itodo, F. W. Abdulrahman, L. G. Hassan, S. A. Maigandi and H. U. Itodo, Physicochemical parameters of Adsorbents from locally sorted H_3PO_4 and $ZnCl_2$ modified Agricultural wastes, *New York Science Journal,* 2010, **3**, 17-24.

RSC Advances Accepted Manuscript

33. A. R. Mohamed, M. Mohammadi and G. N. Darzi, Preparation of carbon molecular sieve from lignocellulosic biomass: A review, *Renewable and sustainable energy reviews*, 2010, **14**, 1591-1599.
34. A.W.M. Ip, J. P. Barford and G. McKay, Production and comparison of high surface area bamboo derived active carbons, *Bioresource technol*., 2008, **99**, 8909-8916.
35. M.-W. Jung, K.-H. Ahn, Y. Lee, K.-P. Kim, J.-S. Rhee, J. T. Park and K.-J. Paeng, Adsorption characteristics of phenol and chlorophenols on granular activated carbons (GAC), *Microchem. J*., 2001, **70**, 123-131.
36. M. Inyang, B. Gao, W. Ding, P. Pullammanappallil, A.R. Zimmerman and X. Cao, Enhanced lead sorption by biochar derived from anaerobically digested sugarcane bagasse, *Separation sci. and tech.*, 2011, **46**, 1950-1956.
37. S. M. Lee and A.P. Davis, Removal of Cu (II) and Cd (II) from aqueous solution by seafood processing waste sludge, *Water Res*., 2001, **35**, 534–540.
38. K. Upendra and M. Bandyopadhyay, Sorption of cadmium from aqueous solution using pretreated rice husk, *Bioresource Technol*., 2006, **97**, 104–109.
39. R. Ayyappan, A. Carmalin Sophia, K. Swaminathan and S. Sandhya, Removal of Pb (II) from aqueous solution using carbon derived from agricultural wastes, *Process Biochem.,* 2005, **40**, 1293-1299.
40. S. Lagergren, About the theory of so-called adsorption of soluble substances, *K. Sven. Vetenskapsakad Handl.,* 1898, **24**, 1–39.
41. Y.S. Ho and G. McKay, Sorption of dye from aqueous solution by peat, *Chem. Eng. J.,* 1978, **70**, 115–124.
42. Y.S. Ho and G. McKay, Pseudo second-order model for sorption processes, *Process Biochem.*, 1999, **34**, 451–465.
43. A.T. Mohd Din, B. H. Hameed and A. L. Ahmad, Batch adsorption of phenol onto Physiochemical-activated coconut shell, *J. Hazard. Mater.,* 2009, **161**, 1522–1529.
44. I. Smiciklas, S. Dimovic, I. Plecas and M. Mitric, Removal of Co^{2+} from aqueous solutions by hydroxyapatite, *Water Res.,* 2006, **40**, 2267–2274.
45. H.M.F. Freundlich, Over the adsorption in solution, *J. Phys. Chem*., 1906, **57**, 385–470.
46. I. Langmuir, The constitution and fundamental properties of solids and liquids, *Journal of the American Chemical Society,* 1916, **38**, 2221–2295.
47. D. Ghosh and G.K. Bhattacharyya, Adsorption of methylene blue on kaolinite, *Appl. Clay Sci.,* 2002, **20**, 295–300.
48. C.H. Giles, D. Smith and A. Huitson, A general treatment and classification of the solute adsorption isotherm. I. Theoretical. *Journal of Colloid and Interface Sci*., 1974, **47**, 755–765.
49. G. Gyananath and D.K. Balhal, Removal of lead (II) from aqueous solutions by adsorption onto chitosan beads, *Cellulose Chem. Technol.*, 2012, **46**, 121-124.

RSC Advances Accepted Manuscript

50. D. Asandei, L. Bulgariu and E. Bobu, lead (II) removal from aqueous solutions by adsorption onto chitosan, *Cellulose Chem. Technol*., 2009, **43**, 211-216.
51. F. Boudrahema, F. Aissani-Benissada and H. Ait-Amarb, Batch sorption dynamics and equilibrium for the removal of lead ions from aqueous phase using activated carbon developed from coffee residue activated with zinc chloride, *Journal of Environmental Management*, 2009, **90**, 3031–3039.
52. A.H. Gedam and R.S.Dongre, Adsorption characterization of Pb (II) ions onto iodate doped chitosan composite: Equilibrium and kinetic studies, *RSC advances,* 2015, **5,** 54188-54201.
53. P. Senthil Kumar, C. Vincent, K. Kirthika and K. Sathish Kumar, Kinetics and equilibrium studies of Pb^{2+} ion removal from aqueous solutions by use of nano-silversol-coated activated carbon, *Brazilian Journal of Chemical Engineering*, 2010, **27**, 339-346.
54. L. Mounia, D. Merabeta, K. Bouzazab and L. Belkhiric, Removal of Pb^{2+} and Zn^{2+} from the aqueous solutions by activated carbon prepared from Dates stone, *Desalination and Water Treatment*, 2010, **16**, 1-8.
55. N. Haloi, H. P. Sarma and P. Chakravarty, Biosorption of lead (II) from water using heartwood charcoal of Areca catechu: equilibrium and kinetics studies, *Appl. Water Sci*., 2013, **3,** 559–565.
56. J. Acharya, J. N. Sahu, C.R. Mohanty and B.C. Meikap, Removal of lead (II) from wastewater by activated carbon developed from Tamarind wood by zinc chloride activation, *Chemical Engineering Journal*, 2009, **149**, 249–262.
57. P. Saueprasearsit, M. Nuanjaraen and M. Chinlapa, Biosorption of Lead (Pb^{2+}) by *Luffa cylindrica* Fiber, *Environmental research J.*, 2010, **4**, 157-166.
58. C. Umpuch, N. Bunmanan, U. Kueasing and P. Kaewsan , Adsorption of Lead from Synthetic Solution Using Luffa Charcoal, *World Academy of Science, Engineering and Technol.*, 2011, **5**, 85-89.

RSC Advances Accepted Manuscript

RSC Advances Accepted Manuscript